The Anomalous Magnetic Moment of The Muon

HE397 – The Standard Model of Particle Physics

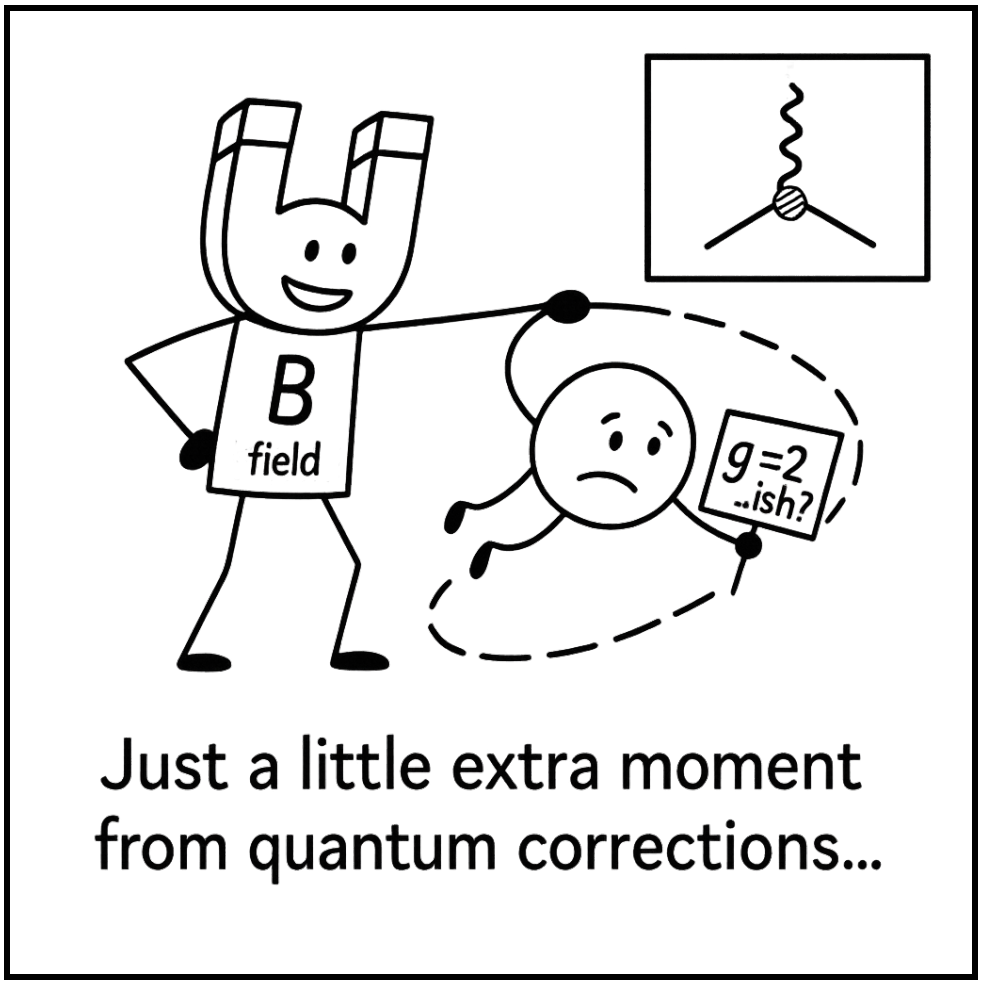

Ananth Ashish Garg B, Abhishek Kundu and Leonard Schwarze

April 15, 2025

Abstract

In this report, we discuss the theoretical background and experimental measurements of the magnetic moment of leptons with an emphasis on the muon. We review the development of the theory from quantum mechanics, where the magnetic moment is an input parameter, to modern quantum field theory and the Standard Model of particle physics. In the latter, perturbative expansions yield predictions from quantum electroweak interactions and the Higgs sector. Hadronic contributions are not accessible perturbatively due to the energy scales involved, and we, therefore, treat them separately. In addition, we discuss the experimental setup mainly used to measure the muon's anomalous magnetic moment and present a series of experiments from Garwin, Lederman and Weinrich to Fermilab.

Contents

1. Introduction

The discrepancy between the theoretical prediction and the experimental measurement of the anomalous magnetic moment of the muon at the E821 experiment in Brookhaven [1] sparked excitement in many physicists that there might be new physics beyond the Standard Model. This excitement was particularly fueled by the confirmation of the result in the experiment E989 at Fermilab [2][3], which increased both the experimental precision of the measurement and the deviation to the value predicted by the Standard Model. With theoretical predictions of incredible precision from quantum electrodynamics [4] and weak theory [5], some scientists became confident that such a discrepancy is best resolved using physics beyond the Standard Model. However, over time it became evident that contributions from quantum chromodynamics have been underestimated, and data driven approaches were the first steps to include the strong sector into the prediction. Despite this, a discrepancy of 4.2σ remained, but new lattice calculations [6, 7] hint that the Standard Model itself may be able to explain the experimental measurement.

In the first part of this work, we review the theory behind the fermionic magnetic moment from quantum mechanics to quantum field theory and the electroweak sector of the Standard Model. We present how quantum corrections lead to modifications of the "classical" prediction from the Dirac equation and how they can, in principle, be calculated in perturbation theory. We also give a brief overview of models beyond the standard model that can influence the magnetic moment of the leptons. In the second part, we discuss the experimental setup used by most experiments, including the ones at Brookhaven and FermiLab, and review the history of experimental predictions and how they compared to theoretical predictions at the time. The third part is explicitly devoted to hadronic contributions. We discuss both the data-driven approach and lattice calculations and present recent results. Finally, in the fourth part, we briefly talk about the upcoming experiment at J-PARC, which aims to independently verify the experiments at Brookhaven and Fermilab.

2. Theory

The purpose of this section is to introduce the theoretical concept related to lepton magnetic moments that are needed to understand the experiments, as well as the connection between experimental measurements and theoretical predictions. As a gentle introduction, we first cover the role of the magnetic moment of spin-1/2 particles in ordinary quantum mechanics before introducing predictions from the Dirac equation and the standard model. For the latter, we will only present results from the electroweak and Higgs sectors, as they can be reasonably easy to understand compared to hadronic contributions. As this is also the case from a historical perspective, we will describe such hadronic effects after discussing the experimental details.

2.1. The Magnetic Moment in Quantum Mechanics

In order to understand how quantum corrections affect the magnetic moment of a lepton in the standard model, it is useful to review how this quantity is expressed in the language of ordinary quantum mechanics. A detailed introduction can be found, for example, in [8]. In this framework, the interaction Hamiltonian of a particle with charge q and an external magnetic field via its spin is given by

$$\mathcal{H}_{\mathrm{I}} = -g\mu\vec{B}\cdot\vec{S}. \tag{2.1}$$

Here, $\vec{B}$ denotes the external magnetic field, $\vec{S} = \frac{\vec{\sigma}}{2}$ is the spin operator for a spin-1/2 particle, $\mu = \frac{q}{2m}$ is the Bohr magneton and g is the gyromagnetic factor. Note that natural units are used, that is, $\hbar = c = 1$. The g-factor indicates how strongly a particle couples to the external magnetic field and is an intrinsic property of the particle itself. In ordinary quantum mechanics, this factor needs to be measured and is not predicted. Together, these quantities define a magnetic moment $\vec{\mu}$:

$$\vec{\mu} = g\mu\vec{S}. \tag{2.2}$$

The time evolution of the pure spin coupling with a magnetic field is given by

$$i\partial_t\psi = -g\frac{q}{2m}\vec{\sigma}\cdot\vec{B}\psi, \tag{2.3}$$

where ψ is a two-component spinor. When $\vec{B} = B\vec{e}_3$, this equation decouples for the two spinor components and results in

$$\psi_\pm \propto \exp\left(\pm i\omega_L t\right) \tag{2.4}$$

with the Larmor frequency $\omega_L = g\mu B$. $\psi_\pm$ are the spinor components $\psi = (\psi_+, \psi_-)^T$.

2.2. Prediction from the Dirac Equation

Interestingly, while in standard quantum mechanics the g-factor is treated as an input parameter, the relativistic generalisation actually predicts this quantity. This can be understood by investigating the Dirac equation in Dirac's original formulation [9]

$$i\partial_t\psi = \left[\vec{\alpha}\left(\hat{p} - q\vec{A}\right) + q\varphi + \beta m\right]\psi. \tag{2.5}$$

Contrary to the previous part, ψ is now a four component spinor, and α and β are 4×4 matrices related to the Clifford algebra $\mathrm{Cl}(1,3)$ via

$$\beta = \gamma^0, \quad \alpha = \gamma^0\gamma^i. \tag{2.6}$$

In Dirac representation, their form is conveniently related to the Pauli matrices

$$\beta = \gamma^0 = \begin{pmatrix} \mathbb{1} & 0 \\ 0 & -\mathbb{1} \end{pmatrix}, \quad \alpha^i = \gamma^0\gamma^i = \begin{pmatrix} 0 & \sigma^i \\ \sigma^i & 0 \end{pmatrix} \tag{2.7}$$

To show how a prediction for g arises from this starting point we wish to express (2.5) in the non-relativistic limit, as, for example, discussed in [10]. This means that we are dealing with a quadratic approximation around $p = 0$ of the mass-shell of the particle. Further, the electromagnetic field should not be able to raise the momentum into a non-relativistic regime. Therefore $E \approx m$ and we can project this energy out using the Ansatz

$$\psi = \psi' \exp(-imt). \tag{2.8}$$

Note that this is essentially a WKB Ansatz in the time coordinate: m sets the largest energy scale and all other energies should satisfy $E' \ll m$ resulting in the corresponding exponentials oscillating much slower than the one we projected out. Splitting the spinor ψ into two two-component spinors $\psi' = (\phi, \chi)^T$ allows us to make the connection to the Pauli equation apparent – plugging this together with (2.8) and (2.6) back into (2.5) we obtain

$$i\partial_t \begin{pmatrix} \phi \\ \chi \end{pmatrix} + m \begin{pmatrix} \phi \\ \chi \end{pmatrix} = \vec{\sigma}\left(\hat{p} - q\vec{A}\right)\begin{pmatrix} \chi \\ \phi \end{pmatrix} + q\varphi \begin{pmatrix} \phi \\ \chi \end{pmatrix} + m \begin{pmatrix} \phi \\ -\chi \end{pmatrix}. \tag{2.9}$$

Looking at the equation for χ we notice that the mass-dependence is still present. Due to (2.8) we know that $i\partial_t\chi$ is subleading and thus can be dropped. The same applies to the electric potential term $q\varphi$. The simplified equation therefore reads

$$\chi = \vec{\sigma}\left(\hat{p} - q\vec{A}\right)\frac{\phi}{2m} \tag{2.10}$$

and we learn that χ is suppressed by $1/m$ with respect to ϕ. Further, the two equations decouple and we obtain the Pauli equation for the leading two-spinor

$$i\partial_t\phi = \vec{\sigma}\left(\hat{p} - q\vec{A}\right)\chi + q\varphi\phi = \left[\left(\vec{\sigma}\left(\hat{p} - q\vec{A}\right)\right)^2 + q\varphi\right]\phi, \tag{2.11}$$

which can be expressed in the form

$$i\partial_t\phi = \left[\left(\hat{p} - q\vec{A}\right)^2 + q\varphi - \frac{q}{2m}\vec{\sigma}\vec{B}\right]\phi \tag{2.12}$$

using the identity

$$(\vec{\sigma}\,\vec{v})\,(\vec{\sigma}\,\vec{w}) = \vec{v}\,\vec{w} + i\vec{\sigma}\,(\vec{v}\times\vec{w}) \tag{2.13}$$

and

$$\left[(\hat{p} - q\vec{A})\times(\hat{p} - q\vec{A})\right]\phi = iq\left(\nabla\times\left(\vec{A}\phi\right) + \vec{A}\times(\nabla\phi)\right) = iq\nabla\times A\phi = iq\vec{B}\phi. \tag{2.14}$$

Comparing the $\vec{\sigma}\vec{B}$ term in (2.12) with the standard quantum mechanics Hamiltonian in (2.1) and using $\vec{S} = \frac{\vec{\sigma}}{2}$ one can read off the relativistic prediction $g = 2$ for any spin-1/2 particle.

2.3. The Magnetic Moment in Quantum Field Theory

The Dirac equation is just the classical equation of motion arising in a field theory. Specifically, the Lagrangian describing a Dirac particle with mass m and charge q minimally coupled to an electromagnetic field is given by

$$\mathcal{L} = \bar{\psi}\left(i\not{D} - m\right)\psi \tag{2.15}$$

with $D^\mu = \partial^\mu - iqA^\mu$. The Dirac equation is then just the Euler-Lagrange equation for this Lagrangian. To understand the influence of quantum effects it is useful to investigate this quantum field theory in the language of Feynman diagrams. In this framework, the pure Dirac equation corresponds to the tree-level prediction of this quantum field theory. Since we know that on tree-level we have $g = 2$, a natural question to ask is how modifications to this value would look like on the level of the Lagrangian and the amplitude. We will now briefly discuss how such corrections arise and how they can be calculated. A rigorous treatment of this can be found in [11, 12, 13]. In principle, due to the Clifford algebra $\mathrm{Cl}(1,3)$, there are five independent spinor bilinears that one can write down:

$$\bar{\psi}\psi \quad \bar{\psi}i\gamma^5\psi \quad \bar{\psi}\gamma^\mu\psi \quad \bar{\psi}\gamma^\mu\gamma^5\psi \quad \bar{\psi}\sigma^{\mu\nu}\psi, \tag{2.16}$$

with $\sigma^{\mu\nu} = \frac{i}{2}\left[\gamma^\mu, \gamma^\nu\right]$. This is because these already count all 16 degrees of freedom that the algebra $\{\gamma^\mu, \gamma^\nu\} = 2\eta^{\mu\nu}\mathbb{1}$ allows for. Of course, arbitrary linear combinations are allowed and all other bilinears like $\bar{\psi}\gamma^5\sigma^{\mu\nu}\psi$ must be reducible to those. The bilinears $\bar{\psi}\psi$ and $\bar{\psi}\gamma^\mu\psi$ are already present in our Lagrangian in (2.15). They describe the mass- and kinetic term of the particle as well as the coupling to the electromgnetic field via the $U(1)$ Noether current $j^\mu = \bar{\psi}\gamma^\mu\psi$. Terms like $\bar{\psi}i\gamma^5\psi$ and $\bar{\psi}\gamma^\mu\gamma^5\psi$ describe pseudoscalars and pseudovectors and should therefore not be included in a theory of quantum electrodynamics with only Dirac particles as leptons. This leaves is with only one bilinear: $\bar{\psi}\sigma^{\mu\nu}\psi$. This turns out to be exactly the term we are looking for! Contracting this with the electromagnetic field strength tensor $F_{\mu\nu}$ yields exactly the desired coupling. Using the definition of the Dirac

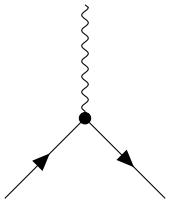

Figure 1: Tree-level diagram for the QED vertex corresponding to $l \to l\gamma$.

matrices γ^μ we can write

$$\sigma^{0i} = i \begin{pmatrix} 0 & \sigma^i \\ \sigma^i & 0 \end{pmatrix}, \quad \sigma^{ij} = \varepsilon^{ijk} \begin{pmatrix} \sigma^k & 0 \\ 0 & \sigma^k \end{pmatrix}. \tag{2.17}$$

Using

$$F_{0i} = E_i, \quad F_{ij} = -\varepsilon_{ijk} B_k \tag{2.18}$$

we thus arrive at

$$\sigma^{\mu\nu} F_{\mu\nu} = 2\sigma^{0i} F_{0i} + \sigma^{ij} F_{ij} = -2 \begin{pmatrix} \vec{\sigma} \cdot \vec{B} & -i\vec{\sigma} \cdot \vec{E} \\ -i\vec{\sigma} \cdot \vec{E} & \vec{\sigma} \cdot B \end{pmatrix} \tag{2.19}$$

and we can see that this contraction can induce a coupling of the lepton spin to the magnetic and electric field. However, there are still several questions left unanswered – For one, we found that the tree-level prediction includes this coupling with $g = 2$, but it is not present in the Lagrangian. Second, $\bar{\psi}\sigma^{\mu\nu}F_{\mu\nu}\psi$ has dimension 5 and should therefore not be present in the bare Lagrangian of any fundamental theory. Both problems can be resolved by applying the Gordon identity (on-shell condition) to the vertex function: We actually do not need to include this term into the bare Lagrangian to generate the coupling. And there are no reasons for why loop diagrams shouldn't generate this term as well. But before talking about quantum effects, let's first see how this term arises in the tree-level amplitude. The diagram of interest is the standard QED vertex describing the scattering $l \to l\gamma$ where l is a lepton and γ is a photon. The diagram is shown in Fig. 1. Translating the diagram in Fig. 1 to the amplitude and amputating the photon polarisation yields

$$\mathcal{M}^\mu_{\text{tree}} = -ie\bar{u}\gamma^\mu u, \tag{2.20}$$

The Gordon identity is [13]

$$\bar{u}(p_1)\gamma^\mu u(p_2) = \bar{u}(p_1)\frac{(p_1+p_2)^\mu}{2m} + i\frac{(p_1-p_2)_\nu}{2m}\sigma^{\mu\nu}u(p_2), \tag{2.21}$$

and applying this to (2.20) yields the coupling

$$\frac{q}{2m} q_\nu \sigma^{\mu\nu} \tag{2.22}$$

with the momentum transfer $q = p_1 - p_2$. Comparing this with the coupling of the spin to the magnetic field in (2.19) then allows us to read off $g = 2$. Any corrections to this

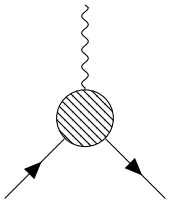

Figure 2: General diagram for the QED vertex corresponding to $l \to l\gamma$. The blob indicates an arbitrary QED interaction.

prediction must also appear with the same tensor structure in the vertex function, as this would correspond to adding the correct interaction Hamiltonian to the dynamics of the theory.

2.4. Higer-order Contributions in Quantum Electrodynamics

The fact that the magnetic moment of a lepton is elevated from an experimental input to a predicted property of a particle when simply generalising standard quantum mechanics to a relativistic version is quite astonishing. It is, however, even more fascinating to see how the full framework of an interacting quantum field theory like quantum electrodynamics (QED) results in additional corrections to the prediction of relativistic quantum mechanics. In this spirit, we will now review the the QED contributions to the lepton magnetic moment through loop diagrams.

Using the language of Feynman diagrams, the general QED process of interest has the form shown in Fig. 2. The blob now indicates that we are talking about any QED process describing the scattering $l \to l\gamma$, including loop diagrams. We wish to write down the general amplitude for this process and restrict it as much as possible using the information we have about this process. To do so, we are allowed to make use of the spinor bilinears allowed by the Clifford algebra and all other Lorentz structures available in the diagram. Because QED is vectorial, the allowed vectorial bilinears are

$$\bar{u}\gamma^\mu u \quad \bar{u}p^\mu u \quad \bar{u}\sigma^{\mu\nu}p_\nu u \tag{2.23}$$

where p stands for any momentum involved in the scattering process. Note that combinations involving $\tilde{\sigma}^{\mu\nu} = \varepsilon^{\mu\nu\rho\tau}\sigma_{\rho\tau}$, which are equivalent to a coupling to the dual field strength tensor $\tilde{F} = \varepsilon^{\mu\nu\rho\tau}F_{\rho\tau}$, are not possible because $\tilde{\sigma}^{\mu\nu} \propto \sigma^{\mu\nu}\gamma^5$. We can now use symmetry information to reduce the number of parameters for a general amplitude. First, we can use translation invariance of the process to relate the momenta involved in the process. Let p_1 and p_2 be the incoming and outgoing lepton momenta and q the photon momentum. Then, translation invariance implies that q is the momentum transfer in the scattering process, i.e. $q = p_2 - p_1$. This relation allows to only use two of the three momenta in the general bilinears:

$$\mathcal{M}^\mu = \bar{u}\left(f_1\gamma^\mu + f_2 p_1^\mu + f_3 p_2^\mu + f_4\sigma^{\mu\nu}p_{1,\nu} + f_5\sigma^{\mu\nu}p_{2,\nu}\right)u. \tag{2.24}$$

A second constraint comes from the Ward identity, or current conservation, which reads

$$q_\mu \mathcal{M}^\mu = 0. \tag{2.25}$$

To translate the Ward identity into relations between the coefficients in (2.24), we need to exploit the relations between the momenta and use on-shell conditions for the photon:

$$q^2 = 0, \quad p_2 q = (q - p_1)\, q = -p_1 q \tag{2.26}$$

and we thus get $f_2 = f_3$. Further,

$$\begin{aligned} q_\mu \sigma^{\mu\nu} p_{1,\nu} &= p_{2,\mu}\sigma^{\mu\nu}p_{1,\nu} - p_{1,\nu}\sigma^{\mu\nu}p_{1,\nu} = p_{2,\mu}\sigma^{\mu\nu}p_{1,\nu} = -p_{1,\mu}\sigma^{\mu\nu}p_{2,\nu} \\ &= p_{2,\mu}\sigma^{\mu\nu}p_{2,\nu} - p_{1,\mu}\sigma^{\mu\nu}p_{2,\nu} = q_\mu \sigma^{\mu\nu} p_{2,\nu} \end{aligned} \tag{2.27}$$

and therefore $f_4 = -f_5$. Using the Gordon identity, a term of the form $p_1 + p_2$ can be expressed via γ^μ and $(p_1 - p_2)_\nu \sigma^{\mu\nu}$. The scalar factors f_i can only depend on scalar quantities and must therefore depend on the squared momenta. Using the on-shell condition for the leptons we arrive at the general form of the matrix element

$$i\mathcal{M}^\mu = (-iq)\bar{u}(p_2)\left[F_1\left(\frac{q^2}{m^2}\right)\gamma^\mu + \frac{i\sigma^{\mu\nu}q_\nu}{2m}F_2\left(\frac{q^2}{m^2}\right)\right]u(p_1). \tag{2.28}$$

For zero momentum transfer the vertex must be measuring the electric charge of the photon and thus $F_1(0) = 1$. This leaves us with an additional contribution in F_2 of the form

$$a \equiv \frac{g-2}{2} = F_2(0), \tag{2.29}$$

where we call a the *anomalous magnetic moment* of the lepton. Conveniently, the two form factors F_1 and F_2 are called the Dirac- and Pauli form factor, corresponding to the couplings they represent.

In fact, (2.28) is the most general form that any amplitude of any QED process can have. This means that if we wish to compute the anomalous magnetic moment in a pure QED process up to arbitrary order, we can always extract F_2 by simply dropping terms proportional to the bilinear $\bar{u}\gamma^\mu u$.

We will now illustrate this for the QED one-loop contribution. The only QED one-loop diagram that contributes to the anomalous magnetic moment of a lepton is shown in Fig. 3. This diagram is the standard QED vertex correction via the exchange of a virtual photon between the external fermion lines. There are three more one-loop diagrams for the process $l \to l\gamma$ that one can write down. These are the electron self-energy and vacuum polarisation diagrams shown in Fig. 4 that are inserted instead of the three external lines of the pure tree-level vertex. However, it turns out that such diagrams do not contribute to the anomalous magnetic moment of the lepton. This is because the loop integrals do not generate the desired tensor structure $\sigma^{\mu\nu}q_\nu$ and are canceled by field renormalisation [12]. The vacuum polarisation loop for example, generates the polarisation tensor [11]

$$\Pi^{\mu\nu} = A\left(q^2, m^2\right)\eta^{\mu\nu} + B\left(q^2, m^2\right)q^\mu q^\nu. \tag{2.30}$$

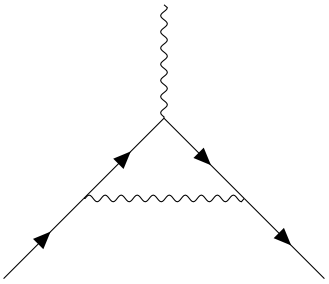

Figure 3: One-loop diagram for QED vertex correction.

Figure 4: Electron self-energy and vacuum polarisation diagrams. Inserting these diagrams into the external legs of the tree-level QED vertex yields a one-loop correction.

The electron self-energy contributes a scalar quantity [11], i.e. the occurring Dirac matrices are contracted via the internal photon propagator. However, none of these indices is contracted with the momentum transfer q. Therefore, the structure $\sigma^{\mu\nu}q_\nu$ will never arise, not even when this portion is embedded into the full $l \to l\gamma$ process. Therefore, the only diagram contributing to $g-2$ one the level of one-loop diagrams in QED is the one shown in Fig. 3.

Because the bare Lagrangian does not contain a $\sigma^{\mu\nu}F_{\mu\nu}$ term, there also exists no renormalisation constant that could account for any divergences for the anomalous magnetic moment. But because QED is renormalisable, the one-loop contributions to the Pauli form factor F_2 must already be finite, showing that divergences coming from one-loop corrections to the external lines must manifest themselves solely in the Dirac form factor.

The vertex correction in Fig. 3 was first evaluated by Julian Schwinger in 1948 [14]. His calculation showed that the one-loop QED correction to the anomalous magnetic moment is given by

$$a_{\text{QED}}^{1-\text{loop}} = \frac{\alpha}{2\pi} \approx 0.00116. \tag{2.31}$$

It is definitely possible to reproduce this result by hand, but evaluating the loop integral is quite involved and requires care. Instead, we provide a `Mathematica` file that evaluates the diagram and isolates the desired tensor structure by dropping $\bar{u}\gamma^\mu u$ bilinears from the amputated matrix element. This makes use of the fact that the one-loop contribution is directly finite. For higher order corrections, proper renormalisation needs to be performed.

Calculating higher-order contributions from pure QED is possible and important for matching the precision of current experimental measurements. Within the framework of the Standard Model, QED corrections account for the largest fraction of the lepton anomalous magnetic moments [15]. The QED contributions for the electron and muon have been calculated up to tenth order and the complete calculation was presented by

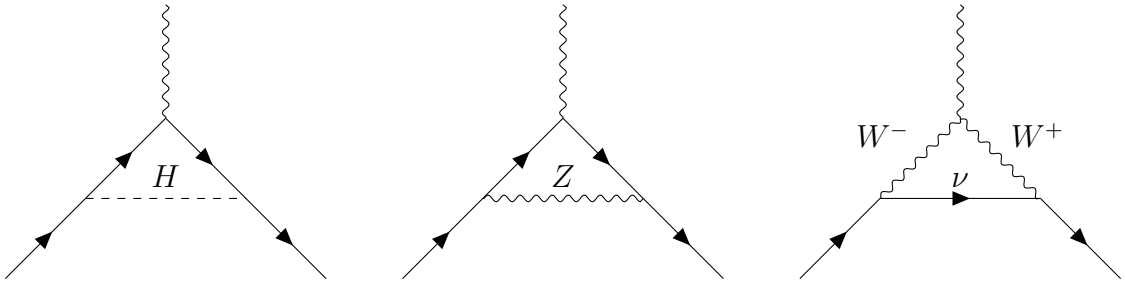

Figure 5: One-loop diagrams contributing to the lepton magnetic moment including weak currents and the Higgs boson.

Aoyama et al. in 2012 [4]. Their result is given by

$$a_{\mu,\mathrm{QED}}^{5-\mathrm{loop}} = 116584718.951(80) \times 10^{-11}. \tag{2.32}$$

The uncertainty splits mainly in four parts: the ratio of the lepton mass ratios, the eigth- and tenth order numerical uncertainties and the uncertainty of the fine structure constant α.

2.5. Weak currents and the Higgs

If quantum electrodynamics were a closed part of the Standard Model in the sense that no other particles could couple to leptons and photons we would be done in the previous section when trying to predict the lepton anomalous magnetic moments. In reality, however, contributions to the magnetic moment of the leptons from other sectors beautifully show how rich the phenomenology of the standard model actually is. One example for this are contributions to the QED vertex correction via weak currents and the Higgs boson. Again, self energy and vacuum polarisation of the external lines cannot have any effect on the magnetic moment. Therefore, we are left with three diagrams on one-loop level, which are shown in Fig. 5. In principle, these diagrams can be evaluated in analogy to the QED contributions. However, one has to be a little more careful here – for one, the vector-axial structure of the weak interactions allow for a more general matrix element. The pseudoscalar and pseudovector spinor bilinears, $\bar{u}i\gamma^5 u$ and $\bar{u}\gamma^5\gamma^\mu$, are now also allowed. However, these bilinears will not contribute to the magnetic moment of the lepton; they just allow for a more general structure of the interaction. Therefore, the coupling we have to extract from these amplitudes is exactly the vector coupling to $\sigma^{\mu\nu}q_\nu$. Second, when working in a general gauge, contributions from the electroweak Goldstone bosons can become important because they are only fully eaten by the gauge bosons in unitary gauge. One could say that their appetite depends on the gauge choice. Including the mixing between the Goldstones and the gauge bosons ensures gauge invariance across arbitrary gauges. Further, even though this is not relevant for the one-loop diagrams, ghost contributions are not negligible, in general, and must also be taken into account.

Again, just like in the QED case, we include `Mathematica` files for each of the three diagrams. The numerical results in the limit $m_\mu \ll m_\mathrm{B}$, where m_B is the mass of the

exchanged boson, are [5]

$$a_{\mu,H}^{1-\text{loop}} \approx 5 \times 10^{-14} \tag{2.33}$$

$$a_{\mu,W}^{1-\text{loop}} = 388.70 \times 10^{-11} \tag{2.34}$$

$$a_{\mu,Z}^{1-\text{loop}} = -193.89 \times 10^{-11}. \tag{2.35}$$

To match the precision of the current QED prediction, two loop corrections are needed in the weak sector, and the total contribution is [16]

$$a_{\mu,\text{Weak}}^{2-\text{loop}} = 153.6(1) \times 10^{-11} \tag{2.36}$$

The reason why two-loop calculations are enough to compare with QED five-loop predictions is the suppression of the diagrams due to the large masses of the W, Z and H.

2.6. The Magnetic Moment Beyond the Standard Model

In the previous sections we have reviewed and presented predictions for the anomalous magnetic moment of the muon. However, it is always useful to be prepared to explain possible discrepancies between theoretical predictions and experimental measurements when confronted with them. The purpose of this part of the document is to say a few words about possible corrections to the magnetic moment of the leptons due to physics beyond the Standard Model. The purpose of this section is not to extensively review BSM models and how they affect $g-2$, but to simply give an idea of what others are working on.

Electric dipole moments (EDM) of leptons are a good candidate for BSM physics that can also show up in measurements of the magnetic moment. If leptons had an EDM larger than predicted by the Standard Model, a misinterpretation of this property in terms of a magnetic moment can show up in experiments using the lepton precession in an external magnetic field: The extra precession might be incorrectly attributed to a shift in the magnetic moment. Using discrepancies between theoretical predictions and experimental measurements, scenarios where an excess or deficiency is predicted can be constraint. In [5], a bound for the EDM of the muon of

$$d_\mu < 2.7 \times 10^{-19} e \cdot \text{cm} \tag{2.37}$$

is given. EDMs are particularly interesting because they provide a measure for $T-$violation and thus also for $CP-$ violation due to the $CPT-$theorem.

Although the Standard Model is incredibly successful in describing the interactions of elementary particles, there is no reason why there should not exist more fundamental forces that we just did not yet account for due to current experimental limitations. Additional gauge bosons can, as discussed in [17], however, contribute to properties like the lepton anomalous magnetic moment, providing windows for experimentally probing and constraining such theories. New bosons would of course not only show up in the

magnetic moments of leptons, in fact some models can be probed in atomic nuclei, for example via the isotope shift of ytterbium [18], making them interesting candidates for BSM models with rich phenomenology.

Dark matter models are difficult to directly probe due to the small interactions with the Standard Model particles. Some models, however, can nonetheless shift observables for which precision measurements are available enough to make the effects detectable. A particular case for which this can happen also touches the realm of a new gauge boson: dark photons as ultralight dark matter candidates. As reported in [19], the Bose enhancement of such dark photons can result in detectable shifts for the magnetic moment of the leptons.

The Higgs boson is the only fundamental scalar in the Standard Model. Due to renormalisation and the running of the bare mass, one expects the mass of the Higgs to be sensitive to the highest scale up to which the Standard Model is valid, unless large amounts of fine tuning protecting the mass from running too much are present. This lead Dugan, Georgi, and Kaplan to the proposition that the Higgs boson might in fact not be fundamental but composite [20]. Many Composite Higgs models can accommodate partner particles to the Standard Model fermions, which they can mix with, and possibly lead to a modification of the magnetic moment of the leptons [21].

Another theory that can account for a rich phenomenology is Supersymmetry (SUSY). Although there is no direct evidence for superpartners in current experiments, some SUSY models like the Minimal Supersymmetric Standard Model (MSSM) provide windows for indirect experimental testing via other observables, one of which being the magnetic moment of the leptons. In [22], an analysis of how loop diagrams involving superpartners can affect the anomalous magnetic moment of the muon is presented.

The SUSY paper [22] leads to an important point that we have not yet discussed, which the authors themselves beautifully stated in the following way:

"Recently a new lattice calculation for the leading order hadronic vacuum polarization (LO HVP) contribution to a_μ^{SM} *[...] has been reported, which, however, was not used in the new theory world average [...]. Consequently, we also do not take this result into account [...]. On the other hand, we are also aware that our conclusions would change substantially if the result presented in [...] turned out to be correct."*

In the previous parts of this section, we only presented contributions from QED and the weak sector. When confronted with experimental measurements of a magnetic moment, however, a prediction by the full Standard Model needs to be made in order to judge the quality of the theory. And, what we did not talk about yet, are contributions from quantum chromodynamics. We will present a review of hadronic contributions after discussing the experiments that measured the anomalous magnetic moment of the muon. But this does not mean that BSM studies like the ones mentioned above are useless. On the contrary, once they are put into context together with experimental measurements and a full Standard Model prediction, such models can be constrained and maybe even excluded, which is exactly the spirit of BSM model building.

3. Experiments

3.1. The Basis

Why do we use the Muon for our experiments?

1. Our experiments for calculating the anomaly in the magnetic moment requires a lepton, but that gives us six choices: the three massive leptons e, μ and τ, and their corresponding neutrinos.

2. Experimentally, producing a high enough luminosity of neutrinos to achieve statistically significant data is quite hard. Detecting any interactions with neutrinos is also hard, reducing the realistic candidates to three.

3. The electron is the lightest lepton and is hence stable with no kinematic option for decay due to lepton number conservation.

4. The τ lepton is quite heavy at 1.78 GeV, but the large mass allows for many different pathways for decay, along with a very short lifetime.

5. Hence, the best candidate is the μ, which has an appreciably long lifespan ($\simeq 2.2\mu s$), which can be increased via boosts. Another convenient fact is that it has one dominant pathway: $e\bar{\nu_e}\nu_\mu$, streamlining experimental design. Pion decay is the source for muon production, which, being a weak process, is maximally parity-violating; hence, we naturally have a polarised muon source.

3.1.1. Particle Dynamics

Note: Under a double Lorentz transformation, we have the following first-order expansions ($x'^\mu = L^\mu_\nu x^\nu$; $x''^\mu = L^\mu_\nu x'^\nu$):

$$\begin{aligned}
\vec{\mathbf{u}}' &= \gamma\left(\delta\vec{\mathbf{v}} + \frac{\gamma-1}{v^2}(\vec{\mathbf{v}}\cdot\delta\vec{\mathbf{v}})\vec{\mathbf{v}}\right) \\
\delta\vec{\theta}' &= \frac{\gamma-1}{v^2}(\delta\vec{\mathbf{v}}\times\vec{\mathbf{v}}) \\
t'' &= t' - \delta\vec{\mathbf{u}}'\cdot\vec{\mathbf{x}}' \\
\delta\vec{\mathbf{x}}'' &= \delta\vec{\mathbf{x}}' + \delta\vec{\theta}'\times\vec{\mathbf{x}}'
\end{aligned} \tag{3.1}$$

Again, our starter equation is the general precession EOM in the non-relativistic limit: $\frac{\partial\vec{P}}{\partial t} = g\frac{e}{2m}\vec{P}\wedge\vec{B}$. This directly gives us the cyclotron frequency: $\vec{\omega}_C = g\frac{e}{2m}\vec{B}$. Since we consider the electric dipole to be 0, the only action of the electric field is acceleration,

$$\delta\vec{\mathbf{u}}' = \frac{e}{m}\vec{\mathbf{E}}'\delta t' \tag{3.2}$$

With the magnetic field providing the precession:

$$\delta\overrightarrow{\mathbf{P}'} = -g\frac{e}{2m}\overrightarrow{\mathbf{B}'} \times \vec{\mathbf{P}}\delta t' \tag{3.3}$$

Considering one more boost, we get:

$$\delta\overrightarrow{\mathbf{P}''} = \delta\overrightarrow{\mathbf{P}'} + \delta\,\vec{\theta}' \times \vec{\mathbf{P}} = -g\frac{e}{2m}(\overrightarrow{\mathbf{B}'} \times \vec{\mathbf{P}})\delta t' + \frac{\gamma-1}{v^2}(\delta\,\vec{\mathbf{v}} \times \vec{\mathbf{v}}) \times \vec{\mathbf{P}} \tag{3.4}$$

Transforming the fields gives us the following:

$$\begin{aligned}
\delta t' &= \gamma\left(\delta t - \frac{\vec{\mathbf{v}} \cdot \delta\vec{\mathbf{x}}}{c^2}\right) = \frac{\delta t}{\gamma} \\
\vec{\mathbf{B}}' &= \gamma\left(\vec{\mathbf{B}} - \frac{\vec{\mathbf{v}} \times \vec{\mathbf{E}}}{c^2}\right) + \frac{\gamma-1}{v^2}(\vec{\mathbf{v}} \cdot \vec{\mathbf{B}})\vec{\mathbf{v}} \\
\vec{\mathbf{E}}' &= \gamma(\vec{\mathbf{E}} + \vec{\mathbf{v}} \times \vec{\mathbf{B}}) + \frac{\gamma-1}{v^2}(\vec{\mathbf{v}} \cdot \vec{\mathbf{E}})\vec{\mathbf{v}}
\end{aligned} \tag{3.5}$$

Finally, replacing everything into the equation for momentum, we find the following extended expression for precession frequency (the first term corresponds to Thomas Precession):

$$\omega_S = \frac{\gamma-1}{v^2}(\frac{\partial\vec{\mathbf{v}}}{\partial t} \times \vec{\mathbf{v}}) - g\frac{e}{2m}\left(\vec{\mathbf{B}} - \frac{\vec{\mathbf{v}} \times \vec{\mathbf{E}}}{c^2} + \frac{\gamma-1}{\gamma v^2}(\vec{\mathbf{v}} \cdot \vec{\mathbf{B}})\vec{\mathbf{v}}\right) \tag{3.6}$$

The boosted Lorentz force equation gives us the acceleration:

$$\frac{\partial\vec{\mathbf{v}}}{\partial t} = \frac{e}{\gamma m}(\vec{\mathbf{E}} + \vec{\mathbf{v}} \times \vec{\mathbf{B}}) - \frac{e}{\gamma m c^2}(\vec{\mathbf{v}} \cdot \vec{\mathbf{E}})\vec{\mathbf{v}} \tag{3.7}$$

Finally, using the identities $(\vec{\mathbf{v}} \times \vec{\mathbf{B}}) \times \vec{\mathbf{v}} = \vec{\mathbf{B}}v^2 - (\vec{\mathbf{v}} \cdot \vec{\mathbf{B}})\vec{\mathbf{v}}$ and $\vec{\mathbf{v}} \times \vec{\mathbf{v}} = 0$, we arrive at:

$$\vec{\omega}_S = \frac{e}{m}\left[\left(\frac{g}{2} - 1 + \frac{1}{\gamma}\right)\vec{\mathbf{B}} - \left(\frac{g}{2} - 1\right)\frac{\gamma\vec{\beta}}{\gamma+1}(\vec{\beta} \cdot \vec{\mathbf{B}}) - \left(\frac{g}{2} - \frac{\gamma}{\gamma+1}\right)\frac{\vec{\beta} \times \vec{\mathbf{E}}}{c}\right] \tag{3.8}$$

To calculate the cyclotron frequency, we assume transverse electric field ($\vec{\mathbf{E}} = 0$), and using the identities $(\vec{\mathbf{v}} \times \vec{\mathbf{E}}) \times \vec{\mathbf{v}} = \vec{\mathbf{E}}v^2 - (\vec{\mathbf{v}} \cdot \vec{\mathbf{B}})\vec{\mathbf{v}} = \vec{\mathbf{E}}v^2$ and $\frac{v^2}{c^2} = \frac{\gamma^2-1}{\gamma^2}$, we get:

$$\vec{\omega}_C = \frac{e}{m}\left[\frac{1}{\gamma}\vec{B} - \frac{\gamma}{\gamma^2-1} \cdot \frac{\vec{\beta} \wedge \vec{E}}{c}\right] \tag{3.9}$$

Thus, the anomalous frequency is [15]:

$$\overrightarrow{\omega_a} = \frac{e}{m}\left[a_\mu\vec{B} - a_\mu\frac{\gamma}{1+\gamma}(\vec{\beta} \cdot \vec{B})\vec{B} - \left(a_\mu + \frac{1}{\gamma^2-1}\right)\frac{\vec{E} \times \vec{\beta}}{c}\right] \tag{3.10}$$

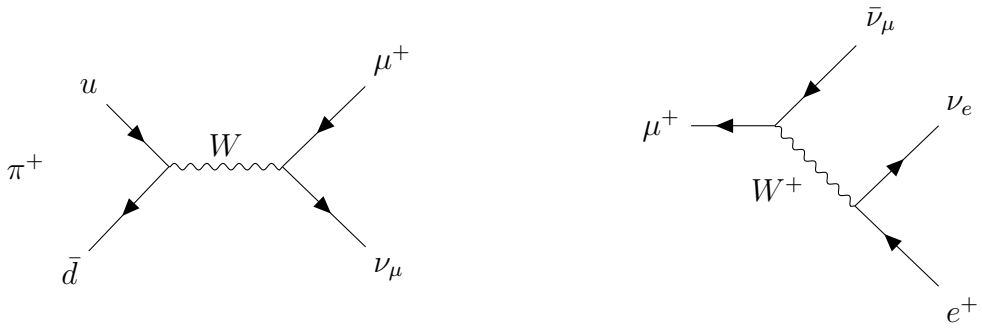

Figure 6: Feynman diagrams of (a) a π^+ decay into an anti-muon and a muon neutrino and (b) an anti-muon decay into a positron, an electron neutrino and a muon antineutrino.

'Magic' Momentum of the Muon

- The extremely complicated general form of the anomalous precession velocity depends on the boost parameter and the orientation of the magnetic field.
- Putting $\vec{\beta} \cdot \vec{B} = 0$: motion perpendicular to the field - takes care of the second term.
- While we don't know the exact value of a_μ, we have an excellent estimate for it- theoretically and experimentally.
- Putting a value of $\gamma = \sqrt{1 + \frac{1}{a_\mu}} \simeq 29.3$ gives us a momentum of 3.094 GeV, with a 10% uncertainty, at which the third term is highly suppressed, thus giving us back a close estimate of the value of the anomaly at zero momentum: which is otherwise experimentally impossible to attain due to breakdown of perturbation theory. [23]

3.2. The Process

1. Since the first experiments on muons, we have used the pion decay as a steady source for muon production: a proton beam bombarded on a target (basic processes $p + p \to p + n + \pi^+$ and $p + n \to p + p + \pi^-$) produces copious amounts of charged pions.
2. Due to their low masses, only the muon and electron channels are kinematically allowed, with the low-mass lepton being heavily suppressed.
3. In the weak decay, the positively charged leptons would be preferentially emitted with right-handed helicity. However, this is vetoed by the massless neutrino and by the conservation of angular momentum (the pion has zero spin).
4. Since the pions are the lightest hadrons, the favoured decay channel is electroweak, thus making sure the muons are longitudinally polarized due to P violation.

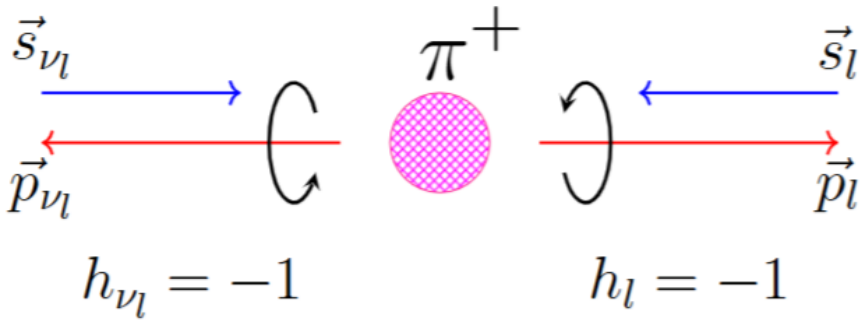

Figure 7: Kinematics of Pion decay [24]

3.2.1. Pion Decay

- The effective Fermi interaction for this process is :

$$\mathcal{L}_{\text{eff,int}} = -\frac{G_\mu}{\sqrt{2}} V_{ud} \left(\bar{\mu}\gamma^\alpha(1-\gamma_5)\nu_\mu\right)\left(\bar{u}\gamma_\alpha(1-\gamma_5)d\right) + \text{h.c.} \tag{3.11}$$

- Pion decay is a parity-violating weak decay where leptons of definite handedness are produced depending on the given charge. Thus, we end up with only one possibility, which we can see in 7:

3.2.2. Muon Decay

The Muon decay process is expressed as follows:

$$\mu^+ \to e^+ \nu_e \bar{\nu_\mu} \tag{3.12}$$

Note: The differential decay width takes its maximum value for the highest energy positron whose momentum is parallel to the muon polarization: once again, this is a result of the parity violation of the V-A nature of weak decay, which prefers to couple to a right-handed positron (or a left-handed electron for a muon jet). The kinematics of the reaction have been pictorially indicated in 8:

Thus, the polarized differential decay probability to find an electron with energy between E and $E+dE$ emitted at an angle between θ and $\theta+d\theta$ ($Q = p_\mu - p_e$, $Q^2 = m_\mu^2 + m_e^2 - 2(p_\mu \cdot p_e)$; $n_\mu = (0, P_\mu)$ in muon rest frame):

$$\frac{\mathrm{d}^2\Gamma}{\mathrm{d}E\mathrm{d}\cos\theta} = \frac{G_\mu^2}{12\pi^3}\frac{p_e}{E_\mu}\left\{Q^2(p_\mu p_e) + 2(Qp_\mu)(Qp_e) - (n_\mu p_e)\left(Q^2 - 2(Qp_e)\right)\right\} \tag{3.13}$$

Again, the effective Lagrangian reads:

$$\mathcal{L}_{\text{eff,int}} = -\frac{G_\mu}{\sqrt{2}} \left(\bar{e}\gamma^\alpha(1-\gamma_5)\nu_e\right)\left(\bar{\nu}_\mu\gamma_\alpha(1-\gamma_5)\mu\right) + \text{h.c.} \tag{3.14}$$

In terms of x = E/W, $x_0 = m_e/\text{W}$, where $\text{W} = (m_\mu^2 + m_e^2)/2m_\mu$ (the maximum energy

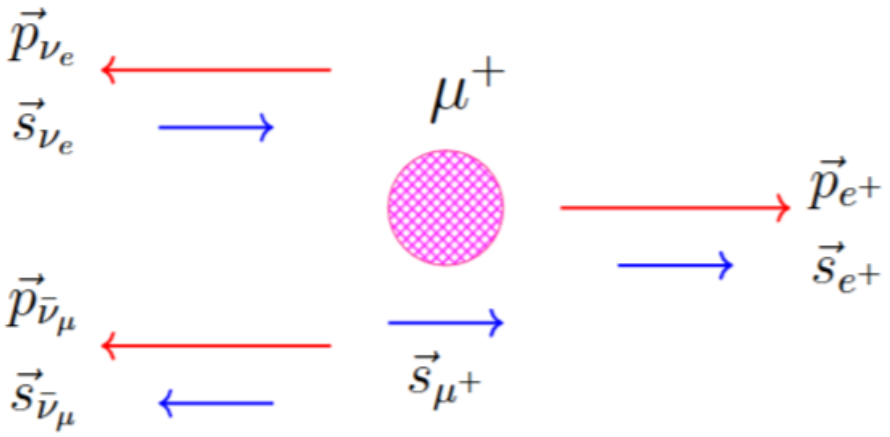

Figure 8: Kinematics of anti-muon decay [24]

the electron can have after the decay):

$$\frac{d^2\Gamma^{\pm}}{dx\, d\cos\theta} = \frac{G_\mu^2 m_\mu^5}{192\pi^3} x^2 \left(3 - 2x \pm P_\mu(2x-1)\cos\theta\right) = \tau_\mu^{-1}\frac{n(E)}{2}\left[1 + a(E)\cos\theta\right] \tag{3.15}$$

where $a(E) = P_\mu\left(\frac{x(2x-1)}{3+x-x^2}\right)$ and $n(E) \propto (x-1)^2(3+x-x^2)$.
As a result, we can see that both the asymmetry and the number density functions are monotonic in the muon rest frame: this implies that decay positrons are overall more likely to be found along the muon spin direction when integrated over energy.

The positron's energy in the laboratory frame, on the other hand, is related to that in the muon's rest frame by: $E = \gamma W(1 - \beta(\mathbf{p}_e^* \cdot \mathbf{p}_e)) = \gamma W(1 + \cos\alpha)$. Now, we can express the differential probability in yet another form:

$$\frac{\partial P}{\partial E} \propto N(E)[1 + \mathcal{P} \cdot A(E)\cos(\omega_a t + \phi)] \tag{3.16}$$

where $\mathcal{P} \simeq 0.95$ and ϕ are the muon's ensemble polarisation and α at injection respectively. Here, $N(E) = \frac{1}{3}(x-1)(4x^2-5x-5)$ and $N(E) = \frac{1+x-8x^2}{4x^2-5x-5}$.

3.2.3. The First Experiment

Garwin, Lederman and Weinrich [25] used a positively charged pion beam of 85 MeV stopped in a carbon absorber and a carbon target to stop the polarized muons emitted from pion decay. They then measured the positron count corrected against the background magnetic field with a scintillating telescope under the principle that a stronger magnetic field would imply a higher Larmor frequency of the muon before the decay. Although this was a very crude setup, it was still enough to estimate the magnetic moment to an accuracy of 10%.

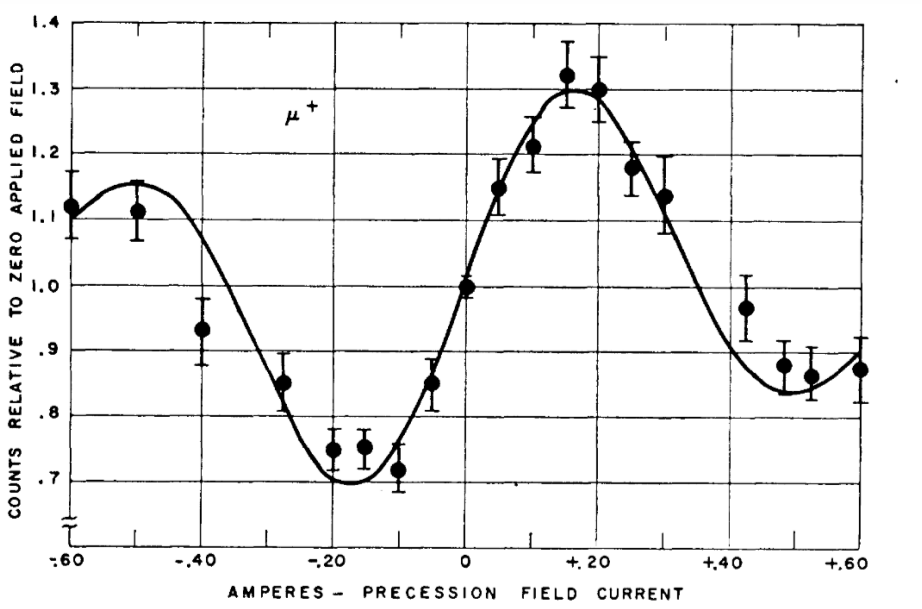

Figure 9: The number of events detected vs. magnetic field plot showed P and C violation in muon decay, and the peak separation for the positron count gave the first measurement of the muon g-factor with a 10% precision, which wasn't enough to observe the magnetic anomaly.

3.3. Experimental Data collection

Observables: $\omega_a = a_\mu \frac{qB}{m}$ (defined earlier, calculated through wiggle plot extrapolation); $\omega_p = 2\mu_p B$ (Larmor precession frequency of the protons in water).

$$a_\mu = \frac{\omega_a}{\omega_p}\frac{\mu_p}{\mu_e}\frac{m_\mu}{m_e}\frac{g_e}{2} \tag{3.17}$$

The other quantities are experimentally well-known constants obtained up to an overall certainty of $\simeq 25$ ppb:

- μ_p: magnetic moment of free proton: 2.79284734462(82) μ_N [26]
- μ_e: magnetic moment of free electron: 1.00115965218059(13) μ_B [27]
- g_e: g factor for electron: 0.00115965218059(13) [27]
- m_e: mass of electron: 0.51099895069(16) MeV [28]
- m_μ: mass of muon: 105.6583755(23) MeV [28]

3.3.1. Wiggle Plots

The number of positrons detected above a certain threshold E_{th} is given by a function: (N_0 and A are experimental parameters obtained by plot-fitting)

$$N(t) = N_0(E_{th})e^{-t/\gamma\tau}(1 + A(E_{th})cos(\omega_a t + \phi)) \tag{3.18}$$

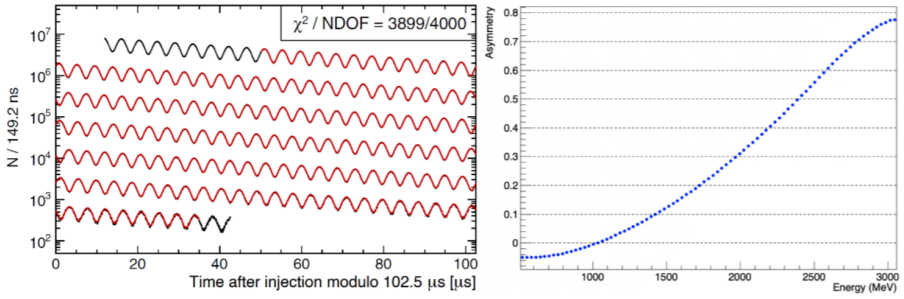

(a) Run-1 T-method wiggle plot. **(b)** A-Method energy weights.

Figure 10: (a) shows the cumulative positron detection events plotted against time; (b) shows the plot of the assymmetry function against energy of the emitted electron

Meanwhile, statistical uncertainty $\delta\omega_a$ is expressed as [15]:

$$\frac{\delta\omega_a}{\omega_a} = \frac{\sqrt{2}}{\omega_a \gamma\tau A\langle P\rangle\sqrt{N}} \tag{3.19}$$

Where $\sqrt{N}$ is due to statistical deviation, A is due to $N^{-1}\partial N/\partial\omega_a \propto A$, the factor $\sqrt{2}/\omega_a\gamma\tau$ accounts for improvement of the accuracy with the number of oscillations, $\langle P\rangle$ is due to polarization. The energy threshold is chosen to minimize the statistical uncertainty of ω_a so that the product NA^2 is maximized.

- Threshold Method or T-Method: all positron events are integrated for energy above a fixed threshold, with equal weights (p(E) = 1). For this method, it was found that the statistical uncertainty is minimal if we integrate energies above 1.7 GeV. (for the FermiLab run 1 Data)
- Asymmetry Weighted Method or A-Method: each positron event is weighted with the asymmetry function A(E) as a function of the positron energy. This technique yields the maximum statistical power, lowering the optimal energy threshold to 1 GeV. We can find the function plot in 10.

3.4. Early Experiments

3.4.1. CERN I

Protons were accelerated in the 600-MeV synchro-cyclotron, scattered against a beryllium target and produced pions; a positively charged muon beam was thus created from pion decays. CERN I aimed to reach 1% accuracy on the anomaly since the theoretical QED corrections had already reached second order ($\simeq$0.001165). The final result showed good agreement with the theory:

$$a_\mu^{exp}(\text{CERN I}) = 0.001162(5) \rightarrow \pm 4300\text{ppm} \tag{3.20}$$

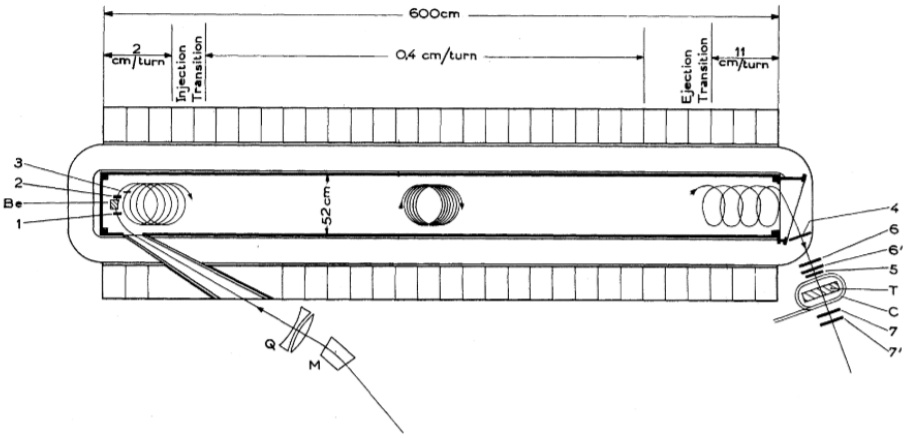

Figure 11: The above image is an overview of the CERN I experimental setup: an anti-muon beam was injected in the dipole magnet, and the coincidence of 1, 2 and 3 counters defined the injection signal; ejected muons stopped in target T, where the stop signal was a coincidence of counters 4, 5, 6, 6 and a veto on counter 7; after the stop signal, the coincidence of 6 6‘ or 7 7‘ defined forward and backwards emitted positrons. [29]

3.4.2. CERN II

Improvements:

- The Storage Ring was introduced, with a diameter of 5m for a 10.5 GeV proton beam
- Higher Luminosity from the Proton Synchrotron made up for protons that did not hit the target and pions that had not decayed, which created an extensive background (namely, the hadronic flash). This also allowed for an optimal initial muon polarization.

The final results showed [30]:

$$a_\mu^{exp}(\text{CERN II}) = 0.00116616(31) \rightarrow \pm 270\text{ppm} \tag{3.21}$$

This data showed a deviation of 1.8σ from the theoretical estimate, which was reconciled with sixth-order QED corrections.

3.4.3. CERN III

Improvements:

- A Storage Ring with a diameter of 14 m was built and immersed in a 1.5 T dipole magnet field, with the beam target moved outside of the Ring so that the hadronic flash could be significantly reduced.

- For the first time, the concept of Magic momentum $|p| = 3.09\text{GeV}$ was used, significantly reducing the uncertainty in the calculations and boosting the mean lifetime of the muons to $64.4\mu s$.

Statistical errors dominated the final results, which were precise enough for three-loop QED corrections and hadronic corrections [23]:

$$\begin{aligned} a_{\mu^+}^{exp}(\text{CERN III}) &= 0.001165911(11) \rightarrow \pm 9\text{ppm} \\ a_{\mu^-}^{exp}(\text{CERN III}) &= 0.001165937(12) \rightarrow \pm 10\text{ppm} \\ a_{\mu}^{exp}(\text{CERN III}) &= 0.001165924(8.5) \rightarrow \pm 7.3\text{ppm} \end{aligned} \tag{3.22}$$

The dilated lifetime allowed a huge dataset collection, so CERN III could verify the CPT theorem, which implies a_{μ^+} and a_{μ^-} should be equal. The experimental value, with 95% CL, was [23]:

$$\frac{a_{\mu^+} - a_{\mu^-}}{a_\mu} \in [-50, 6] \times 10^{-6} \tag{3.23}$$

BNL data will later support this conclusion, with a much lower uncertainty owing to the larger sample size.

3.4.4. E821 Experiment @Brookhaven

Improvements over CERN III:

- Higher rate of muons: BNL reached a dataset size 20 times as large as for CERN III, which was possible because the muon flux could be increased by approximately a factor of 400 thanks to the high luminosity of AGS (Alternating Gradient Synchrotron).
- A better way of injection: in CERN III, pions were injected in the Ring and completed one orbit before impacting the exterior wall of the inflector. Thus, muons emitted by pions were limited in number; in BNL, pions were allowed to decay in a long ($\simeq$ 80 m) channel upstream of the storage ring, and then the muon beam was directly injected into the Ring.
- The storage ring with a diameter of 7 m was composed of three continuously wound superconductors instead of the 40 independent bending magnets of CERN III, which allowed the magnetic field to be much more uniform (an increase by a factor of 3 in uniformity).

The final results for BNL were [1]:

$$
\begin{aligned}
a_{\mu^+}^{exp}(\text{BNL}) &= 0.0011659204(9) \rightarrow \pm 0.73\text{ppm} \\
a_{\mu^-}^{exp}(\text{BNL}) &= 0.0011659214(9) \rightarrow \pm 0.72\text{ppm} \\
a_{\mu}^{exp}(\text{BNL}) &= 0.00116592080(63) \rightarrow \pm 0.54\text{ppm}
\end{aligned} \tag{3.24}
$$

The data had a deviation from the then theoretical value that included 5-loop QED calculations and the second-order of EW and hadronic loops: $a_\mu^{exp}(\text{BNL}) - a_\mu^{th} = 268.6(72.4) \times 10^{-11} \simeq 3.7\sigma$, implying BSM contributions.

3.4.5. E989 Experiment @FermiLab

Improvements:

- The average rate of muon injection was 12 Hz, compared to only 4.4 Hz at BNL, allowing a much larger dataset for calculation.
- A longer pion decay line ($\simeq$ 2 km), ensuring a highly reduced hadronic flash from pion decay to neutrons.
- A high precision laser calibration system to continuously re-calibrate the detectors, which reduces systematic error on ω_a.
- Hardware upgrades (Edge shims, wedge shims, top hats and steel foils) to increase the magnetic field uniformity by a factor of 3 wrt. BNL.

The experiment protocol was as follows:

- Protons are accelerated in the linear accelerator Linac to 400 MeV and injected into the Booster, which accelerates protons to 8 GeV.
- The Recycler groups the protons into bunches with approximately 4×10^{12} particles and a temporal width of $\simeq$ 120 ns.
- Each bunch propagates to the AP0 target hall, where protons collide on a cylindrical core made from a nickel-chromium-iron alloy (Inconel-60).
- An electrostatic lithium lens focuses the secondary beam, which then goes through a momentum filter that selects a beam of particles at the magic momentum.
- In the Delivery Ring, spatial separation is created between the pions (together with the emitted muons) and protons, which are more massive and therefore have a smaller Lorentz boost factor given the same momentum. By the time the bunches exit the Ring, they travel $\simeq$ 2km, enough for all pions to decay into muons (decay length $\simeq$ 170m).

- Finally, an inflector magnet cancels the fringe field of the Ring itself, which otherwise would deflect the beam into the magnetic iron and reduce injection efficiency.

The data from Run 1 and Run 2/3 are as follows [2]; [3]:

$$\begin{aligned} a_\mu^{exp}(\text{Fermilab, 2021}) &= 0.00116592040(54) \rightarrow \pm 0.46\text{ppm} \\ a_\mu^{exp}(\text{FermiLab, 2023}) &= 0.00116592057(25) \rightarrow \pm 0.21\text{ppm} \end{aligned} \tag{3.25}$$

These data are consistent with the BNL data, with a deviation of 4.2σ, which, although lower than the discovery threshold of 5σ, is still outlier enough for many physicists to consider BSM theories as candidates to solve the mystery.

3.5. Experimental Summary

Experiment	Particles	$a_\mu \times 10^{11}$	Precision [ppm]
CERN I	μ^+	$1162(5) \times 10^5$	4300
CERN II	μ^+, μ^-	$116616(31) \times 10^3$	270
CERN III	μ^+, μ^-	116592400(850)	7.3
BNL	μ^+, μ^-	116592080(63)	0.54
FNAL	μ^+	116592055(24)	0.20
Average (BNL + FNAL)		116592059(22)	0.19

Table 1: Summary of experiments measuring the muon anomalous magnetic moment.[1][3][23][29][30]

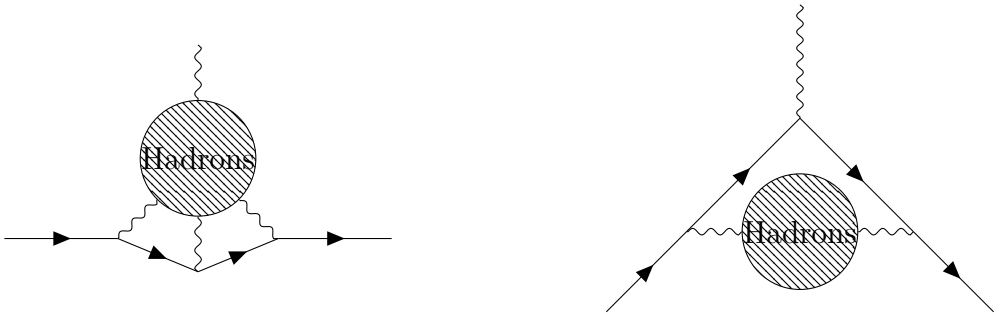

Figure 12: Diagrams for contributions from hadronic light by light scattering (left) and hadronic vacuum polarisation (right).

4. Hadronic contributions

The electromagnetic and weak contributions to the muon's anomalous magnetic moment are the major contributions. However, scope of resolution for the tension between the standard model value and experiment is mostly from the hadronic sectors. Hadronic contributions to the anomalous magnetic moment come from Hadronic Vacuum Polarization and Hadronic Light by Light contributions. Hadronic Vacuum polarization is the hadronic correction to the photon propagator via quark antiquark pairs interacting through strong interactions. The diagrams for these processes are shown in Fig. 12.

4.1. Calculation of Hadronic vacuum Polarization

In order to calculate the Hadronic vacuum polarization, we need to understand the effect of the Hadrons on the photon propagator. We first assume that the addition of one hadron loop gives a term like $\Pi_{\mu\nu}(Q)$. This would change the propagator in the following fashion:

$$\frac{1}{q^2}g_{\mu\nu} \rightarrow \frac{1}{q^2}g_{\mu\lambda}\Pi_{\lambda\rho}(q)\frac{1}{q^2}g_{\rho\nu}$$

. As the new propagator has to still obey the Ward identities we have that

$$q^\mu \Pi_{\mu\nu}(q) = 0$$

This constrains $\Pi_{\mu\nu}$ to have the form

$$(-Qg_{\mu\nu} + Q_\mu Q_\nu)\Pi(Q^2)$$

. This now changes the photon propagator as

$$D(q) = \frac{1}{q^2} + \frac{1}{q^2}\Pi(q^2)\frac{1}{q^2} + \frac{1}{q^2}\Pi(q^2)\frac{1}{q^2}\Pi(q^2)\frac{1}{q^2} + \cdots$$

Which gives the expression

$$D_{\mu\nu}(q) = \frac{-ig_{\mu\nu}}{q^2\left(1 - \Pi(q^2)\right)} \tag{4.1}$$

So, in order to get the contribution of HVP, we must try to get $\Pi(Q^2)$.In the next section, we try to get this value.

4.2. The Data Driven Method

In order to get the contribution of $\Pi(Q^2)$, we use the Cauchy integral formula

$$f(a) = \frac{1}{2\pi i} \oint_\gamma \frac{f(z)}{z-a}\, dz \tag{4.2}$$

When f(z) is analytic in the region enclosed by the contour γ. In the case of propagator for fields, we have a singularity at the mass of the particle described by the field. For composite particles, the pole changes to a branch cut. For the case of $\Pi(q^2)$ there is a branch cut from the lowest possible mass of the hadron. We take a contour that goes above and below the branch cut. The difference in the value above and below the branch cut is equal to the imaginary part of the function in this case. So we have

$$\Pi(q^2) = \frac{1}{\pi} \int_{s_0}^{\infty} ds\, \frac{\mathrm{Im}\,\Pi(s)}{s - q^2 - i\epsilon} \tag{4.3}$$

The function $\Pi(q^2)$ is divergent for large q. So, it is more useful to take the integral formula for the function after dividing by q^2 to get

$$\Pi(q^2) = \frac{q^2}{\pi} \int_{s_0}^{\infty} ds\, \frac{2\mathrm{Im}\,\Pi(s)}{s(s - q^2 - i\epsilon)} \tag{4.4}$$

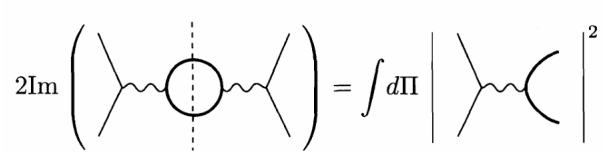

Now, in order to get the term $\mathrm{Im}\Pi(s)$ we use the **Optical Theorem** [31]. The optical theorem states that this difference is equal to the cross section of $\gamma^* \to hadrons$. The optical theorem is

$$-i\left[\mathcal{M}(a \to b) - \mathcal{M}^*(b \to a)\right] = \sum_f \int d\Pi_f\, \mathcal{M}^*(b \to f)\, \mathcal{M}(a \to f) \tag{4.5}$$

Here a and b are γ^* and the final states f are the hadrons.We can use the amplitude of electron positron scattering to hadrons in this formula to compute the function $\Pi(s)$. This is where the name "Data Driven Approach" comes from. We use the data of the collision cross sections of electron positron pair going to hadrons in the computation of the muon anomalous magnetic moment. From the optical theorem, we have

$$\mathrm{Im}\Pi(s) \propto e^+e^- \to \text{hadrons}.$$

Taking the appropriate normalization, we have

$$\mathrm{Im}\Pi(Q^2) = \frac{\alpha}{3} R(Q^2)$$

, where

$$R(Q^2) = \frac{e^+e^- \to hadrons}{e^+e^- \to \mu^+\mu^-}. \tag{4.6}$$

If the contribution from the free photon reads

$$a_\mu \sim \int \frac{d^4q}{(2\pi)^4} \frac{1}{q^2} \times F(q^2, m_\mu), \tag{4.7}$$

then the Taylor series expansion of the photon propagator with hadronic contributions yields

$$a_\mu^{\mathrm{HVP}} \sim \int \frac{d^4q}{(2\pi)^4} \frac{1}{q^2} \Pi(q^2) \times F(q^2, m_\mu). \tag{4.8}$$

Now we substitute $\Pi(q^2)$ with the value we have from the Cauchy integral formula to rewrite the HVP contribution as

$$a_\mu^{\mathrm{HVP}} = \int \frac{d^4q}{(2\pi)^4} \left[\int ds \, \frac{\mathrm{Im}\,\Pi(s)}{s(s-q^2)} \right] \times F(q^2, m_\mu)$$

Now, we group the terms in the denominator and the terms from the fermions to write a kernel function. This kernel function is sometimes modified to give higher weights to lower momenta. Writing in terms of a kernel function and using the relation between $\mathrm{Im}\Pi(s)$ and R(s) we have

$$a_\mu^{\mathrm{HVP}} = \left(\frac{\alpha m_\mu}{3\pi}\right)^2 \int_{s_0}^{\infty} \frac{ds}{s^2} K(s) R(s) \tag{4.9}$$

We take s_0 to be the mass of the pion as it is the lowest energy the hadrons can have The kernel function is given by

$$K(s) = \frac{x^2}{2}(2 - x^2) + \frac{(1+x^2)(1+x)^2}{x^2} \left(\log(1+x) - x + \frac{x^2}{2} \right) + \frac{1+x}{1-x} x^2 \log x, \tag{4.10}$$

where

$$x = \frac{1 - \beta_\mu}{1 + \beta_\mu} \tag{4.11}$$

and

$$\beta_\mu = \sqrt{1 - \frac{4m_\mu^2}{s}}. \tag{4.12}$$

Using this approach and similar data driven approaches for HLbL, the values of the muon anomalous magnetic moment up to different orders along with lattice data give the values that are shown in Tab. 2.

Contribution	**Value** $\times 10^{11}$
HVP LO (e^+e^-)	6931(40)
HVP NLO (e^+e^-)	−98.3(7)
HVP NNLO (e^+e^-)	12.4(1)
HVP LO (lattice, *udsc*)	7116(184)
HLbL (phenomenology)	92(19)
HLbL NLO (phenomenology)	2(1)
HLbL (lattice, *uds*)	79(35)
HLbL (phenomenology + lattice)	90(17)
QED	116 584 718.931(104)
Electroweak	153.6(1.0)
HVP (e^+e^-, LO + NLO + NNLO)	6845(40)
HLbL (phenomenology + lattice + NLO)	92(18)
Total SM Value	**116 591 810(43)**

Table 2: HVP and HLbL contributions to a_μ and total SM prediction including them [32]

4.3. Calculation on the Lattice.

The calculation of $\Pi(Q^2)$ can be done on the lattice. The discussion follows from [7]. The calculation begins by looking at the correlator of the electromagnetic current

$$C_{\mu\nu}^{(N_f)}(x) = \left\langle j_\mu^{(N_f)}(x) j_\nu^{(N_f)}(0) \right\rangle$$

Once we have this current, we take a Fourier transform to Vacuum Polarization tensor,

$$\Pi_{\mu\nu}^{(N_f)}(Q) = \int d^4x \, e^{iQ\cdot x} C_{\mu\nu}^{(N_f)}(x) \tag{4.13}$$

In order to get the contribution to the muon anomalous magnetic moment, we need to take an integral over the momentum carried by the photon. So, we have,

$$a_\mu^{\text{HVP, LO}} = \left(\frac{\alpha}{\pi}\right)^2 \int_0^\infty dQ^2 f(Q^2) \widehat{\Pi}(Q^2) \tag{4.14}$$

with

$$f(Q^2) = \frac{m_\mu^2 Q^2 Z^3 (1 - Q^2 Z)}{1 + m_\mu^2 Q^2 Z^2}, \quad \widehat{\Pi}(Q^2) \equiv 4\pi^2 \left[\Pi(0) - \Pi(Q^2)\right] \tag{4.15}$$

where

$$Z = -\frac{Q^2 - \sqrt{Q^4 + 4m_\mu^2 Q^2}}{2m_\mu^2 Q^2} \tag{4.16}$$

As mentioned above, the function $\Pi(Q^2)$ can be written in the form

$$(-Q^2 \delta_{\mu\nu} + Q_\mu Q_\nu)\Pi(Q^2).$$

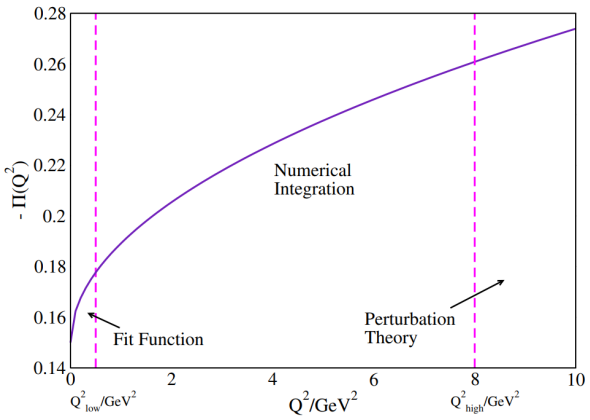

Figure 13: Divsion of the integral into various sectors [7]

We use this to write

$$\Pi(Q^2) = \frac{\sum_\mu \Pi_{\mu\mu}}{3Q^2}$$

Once we have this, we can compute the anomalous moment. The kernel function f(Q^2) peaks at low momenta, about one quarter the mass of the pion. The value of $\Pi(Q^2)$ cannot be computed for very low momenta as lattice extensions of about 10fm would be required. So, we try to extrapolate the data from the low lying accessible momenta to get the value in very low momentum regime. We divide the integral into

$$\begin{aligned} a_\mu^{\text{HVP, LO}} &= I_0 + I_1 + I_2, \\ I_0 &= \left(\frac{\alpha}{\pi}\right)^2 \int_0^{Q^2_{\text{low}}} dQ^2\, f(Q^2) \times \hat{\Pi}(Q^2), \\ I_1 &= \left(\frac{\alpha}{\pi}\right)^2 \int_{Q^2_{\text{low}}}^{Q^2_{\text{high}}} dQ^2\, f(Q^2) \times \hat{\Pi}(Q^2), \\ I_2 &= \left(\frac{\alpha}{\pi}\right)^2 \int_{Q^2_{\text{high}}}^{\infty} dQ^2\, f(Q^2) \times \hat{\Pi}_{\text{pert}}(Q^2), \end{aligned}$$

which is graphically depicted in Fig. 13. The calculation for momenta above Q_{high} is done using perturbation theory. Lattice calculations give the value between Q_{low} and Q_{high}. For the low momentum regime, which gives the highest contribution, we use extrapolation methods.

The first extrapolation method is to use Pade approximants, which are given by

$$\Pi_{[N,M]}(Q^2) = \Pi(0) + \frac{\sum_{i=1}^{N} a_i Q^{2i}}{1 + \sum_{i=1}^{M} b_i Q^{2i}} \tag{4.17}$$

The second method that is used is that of time moments. We look at the component of the Vacuum Polarization tensor with identical spatial indices with $Q^\mu = (\omega, 0, 0, 0)$. We have

$$\Pi_{kk}(Q) = Q^2\Pi(Q^2) = \omega^2\Pi(\omega^2) \tag{4.18}$$

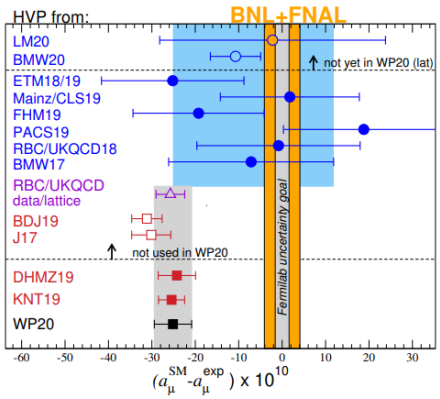

Figure 14: Comparison of Lattice results to experimental data [32]

We can write this term in terms of the correlator as

$$\omega^2 \Pi(\omega^2) = \int d^4x \, e^{iQ\cdot x} C_{kk}(x)$$

We can average over all spatial directions to get

$$\mathcal{C}(x_0) = -\frac{1}{3}\sum_{k=1}^{3} \int d^3x \, C_{kk}(x) \tag{4.19}$$

As the dot product $Q \cdot x = \omega . x_0$ we have the integral in the RHS of the $\Pi(\omega^2)$ equation as

$$-\int dx_0 \, e^{i\omega x_0} \mathcal{C}(x_0) \tag{4.20}$$

We write the moments of this function now to get

$$G_{2n} \equiv \int_{-\infty}^{\infty} dx_0 \, x_0^{2n} \mathcal{C}(x_0) = (-1)^{n+1} \frac{\partial^{2n}}{\partial \omega^{2n}} \left(\omega^2 \Pi(\omega^2)\right)_{\omega=0} \tag{4.21}$$

Now, we get $\Pi(Q^2)$ from this as

$$\Pi(Q^2) = \Pi_0 + \sum_{n=1}^{\infty} \Pi_n Q^{2n} \tag{4.22}$$

With

$$\Pi_0 = \Pi(0) = -\frac{1}{2} G_2, \quad \Pi_n = \frac{(-1)^{n+1}}{(2n+2)!} G_{2n+2} \tag{4.23}$$

We can construct a Pade approximation using these time moments.

Using these methods, many lattice studies have been performed. The results from the data and their comparison with experiment can be seen in Fig. 14. The data points are from the lattice studies conducted by various groups. The details of the lattice methods used are given in Tab. 3. Here, the column titled fermions is for the different fermion

Collaboration	N_f	$a_\mu^{\text{HVP, LO}} \times 10^{10}$	Fermion	$\hat{\Pi}(Q^2)$
ETM-18/19	2+1+1	692.1(16.3)	tmQCD	TMR
FHM-19	2+1+1	699(15)	HISQ	Padé w. Moments/TMR
BMW-17	2+1+1	711.1(7.5)(17.5)	Stout4S	TMR
HPQCD-16	2+1+1	667(16)(13)	HISQ	Padé w. Moments
ETM-13	2+1+1	674(21)(18)*	tmQCD	VMD
Mainz/CLS-19	2+1	720.0(12.4)(9.0)	Clover	TMR
PACS-19	2+1	$737(9)^{+13}_{-8}$	StoutW	TMR/Padé
RBC/UKQCD-18	2+1	717.4(16.3)(9.2)	DWF	TMR
Mainz-17	2	$654(32)^{(+21)}_{(-23)}$	Clover	TMR
KNT-19	pheno.	692.8(2.4)	–	dispersion
DHMZ-19	pheno.	694.0(4.0)	–	dispersion
BDJ-19	pheno.	687.1(3.0)	–	dispersion
FJ-17	pheno.	688.1(4.1)	–	dispersion
RBC/UKQCD-18	lat.+pheno.	692.5(1.4)(2.3)	DWF	TMR + disp.

Table 3: Results from Various lattice calculations [7]

actions which are used in the computation of the correlator. HISQ is highly improved staggered quarks. Clover is improved Wilson fermions. DW stands for Domain Wall fermions. TM is for twisted mass fermions.

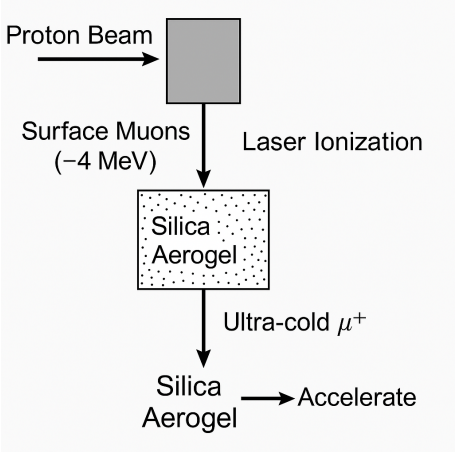

Figure 15: Schematic of the proposed J-PARC experiment.

5. Future: JPARC

The anomalous magnetic moment of the muon currently has a 4.2σ deviation of the experimental data from the Standard Model predictions. This is a solid indicator for BSM physics. However, the difference is still not statistically significant enough to consider it an anomaly. More precise measurements could remove the tension or provide concrete evidence for an anomaly. The new experiment at J-PARC [33] precisely aims at doing this. It showcases a new procedure to measure the magnetic moment of the electron at low energies, without high boosts or an electric field. It uses muonium atoms to produce thermalized muons which are then accelerated to measure the magnetic moment.

5.1. The Setup

Fig. 15 shows the schematic for the production of muons in the J-PARC experiment. Following is a condensed procedure for the experiment:

1. The protons hit a graphite target, and the produced pions come to rest on the graphite.
2. The pions at rest form (thermalised) surface muons with very low energy.
3. The surface muons go into a silica gel, forming muonium(μ^+e^-) atoms.
4. The muonium is excited by a laser and the muons are accelerated into to the storage ring.

Unlike the other experiments, the experiment at J-PARC does not use electric fields. The higher-energy muons in the FermiLab and Brookhaven experiments ($\simeq$3GeV) need an electric field to stop the muons from moving in directions perpendicular to the desired direction of motion. As the muons in J-PARC are much slower, they can get away with not needing this. As there is no electric field, the angular momentum in the direction perpendicular to the magnetic field is solely due to the muon's electric dipole moment.

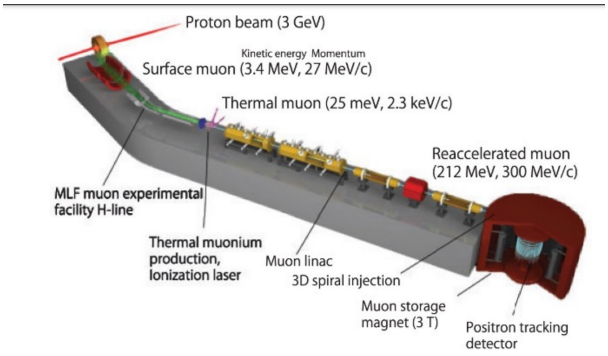

Figure 16: A schematic of the setup and the muon energy as the bunches move through the chambers

Therefore, this gives us an opportunity to test $T-$violation in the Standard Model through the electric dipole moment of the muon.

5.2. Details of the experiment

Muons are produced by injecting a proton beam of energy 3 GeV with a power of 1 MW into a 2 cm thick graphite target. Surface muons of momentum 27 MeV/c are extracted. These are then sent to the silicon target where they form muonium atoms, ionized by a laser, and thermal muons are produced. These are then re-accelerated to 300 MeV/c.

The re-acceleration of thermal muons allows for a low-emittance muon source, that is, the muon beam expands less than in conventional muon production. Eventually, this makes the injection of the muons into the storage magnet easier. Eventually, because of this, the storage magnet can be much more compact than the one used in BNL E821 and FNAL E989. Using a new storage ring makes the observations independent of the ones at Brookhaven and Fermilab, which shared the same storage ring.

6. Conclusion

We reviewed the theory and experimental measurements of the magnetic moment of leptons with an emphasis on the muon. We found that in ordinary quantum mechanics, the magnetic moment of a particle is an input parameter that has to be experimentally determined. On the same lines, the relativistic generalisation of the Dirac equation provides the first prediction of $g = 2$ for any spin-1/2 particle. In the framework of quantum field theory, loop diagrams refine this prediction and, therefore, provide a window for experimental testing of the Standard Model in this aspect. We found that the corrections from electroweak theory can be calculated to extraordinary precision, but they alone are not enough to explain the anomalous moment as accurately as found with modern experiments. Rather, a confident prediction including hadronic contributions must be included as well. In 2023, Fermilab reported a deviation from the Standard Model prediction of 4.2σ. There are many possible solutions to resolve this discrepancy using physics beyond the standard model. However, we have seen that recent lattice calculations are also able to accommodate the experimental measurement or at least reduce the discrepancy within their errors. Future experiments like the one at J-PARC can independently test the previous experiments at Brookhaven and Fermilab and can shed light on possible systematic errors in these experiments.

References

[1] G. W. Bennett et al. "Final report of the E821 muon anomalous magnetic moment measurement at BNL". In: *Phys. Rev. D* 73 (7 Apr. 2006), p. 072003. DOI: 10.1103/PhysRevD.73.072003. URL: https://link.aps.org/doi/10.1103/PhysRevD.73.072003.

[2] B. Abi et al. "Measurement of the Positive Muon Anomalous Magnetic Moment to 0.46 ppm". In: *Phys. Rev. Lett.* 126 (14 Apr. 2021), p. 141801. DOI: 10.1103/PhysRevLett.126.141801. URL: https://link.aps.org/doi/10.1103/PhysRevLett.126.141801.

[3] D. P. Aguillard et al. "Measurement of the Positive Muon Anomalous Magnetic Moment to 0.20 ppm". In: *Phys. Rev. Lett.* 131 (16 Oct. 2023), p. 161802. DOI: 10.1103/PhysRevLett.131.161802. URL: https://link.aps.org/doi/10.1103/PhysRevLett.131.161802.

[4] Tatsumi Aoyama, Masashi Hayakawa, Toichiro Kinoshita, and Makiko Nio. "Complete Tenth-Order QED Contribution to the Muon g-2". In: *Phys. Rev. Lett.* 109 (2012), p. 111808. DOI: 10.1103/PhysRevLett.109.111808. arXiv: 1205.5370 [hep-ph].

[5] Fred Jegerlehner and Andreas Nyffeler. "The Muon g-2". In: *Phys. Rept.* 477 (2009), pp. 1–110. DOI: 10.1016/j.physrep.2009.04.003. arXiv: 0902.3360 [hep-ph].

[6] Sz. Borsanyi et al. "Leading hadronic contribution to the muon magnetic moment from lattice QCD". In: *Nature* 593.7857 (2021), pp. 51–55. DOI: 10.1038/s41586-021-03418-1. arXiv: 2002.12347 [hep-lat].

[7] T. Aoyama et al. "The anomalous magnetic moment of the muon in the Standard Model". In: *Phys. Rept.* 887 (2020), pp. 1–166. DOI: 10.1016/j.physrep.2020.07.006. arXiv: 2006.04822 [hep-ph].

[8] Ramamurti Shankar. *Principles of quantum mechanics*. New York, NY: Plenum, 1980. URL: https://cds.cern.ch/record/102017.

[9] Paul A. M. Dirac. "The quantum theory of the electron". In: *Proc. Roy. Soc. Lond. A* 117 (1928), pp. 610–624. DOI: 10.1098/rspa.1928.0023.

[10] Walter Greiner. *Relativistic Quantum Mechanics. Wave Equations*. Berlin: Springer, 1997. DOI: 10.1007/978-3-662-03425-5.

[11] Matthew D. Schwartz. *Quantum Field Theory and the Standard Model*. Cambridge University Press, Mar. 2014.

[12] Steven Weinberg. *The Quantum theory of fields. Vol. 1: Foundations*. Cambridge University Press, June 2005. DOI: 10.1017/CBO9781139644167.

[13] Michael Kachelriess. *Quantum Fields: From the Hubble to the Planck Scale*. Oxford Graduate Texts. Oxford University Press, Oct. 2017. DOI: 10.1093/oso/9780198802877.001.0001.

[14] Julian S. Schwinger. "On Quantum electrodynamics and the magnetic moment of the electron". In: *Phys. Rev.* 73 (1948), pp. 416–417. DOI: 10.1103/PhysRev.73.416.

[15] Friedrich Jegerlehner. *The Anomalous Magnetic Moment of the Muon*. Vol. 274. Cham: Springer, 2017. DOI: 10.1007/978-3-319-63577-4.

[16] C. Gnendiger, D. Stöckinger, and H. Stöckinger-Kim. "The electroweak contributions to $(g-2)_\mu$ after the Higgs boson mass measurement". In: *Phys. Rev. D* 88 (2013), p. 053005. DOI: 10.1103/PhysRevD.88.053005. arXiv: 1306.5546 [hep-ph].

[17] Dan Hooper, Joaquim Iguaz Juan, and Pasquale D. Serpico. "Signals of a new gauge boson from IceCube and the muon g-2". In: *Phys. Rev. D* 108.2 (2023), p. 023007. DOI: 10.1103/PhysRevD.108.023007. arXiv: 2302.03571 [astro-ph.HE].

[18] Menno Door et al. "Probing New Bosons and Nuclear Structure with Ytterbium Isotope Shifts". In: *Phys. Rev. Lett.* 134 (6 Feb. 2025), p. 063002. DOI: 10.1103/PhysRevLett.134.063002. URL: https://link.aps.org/doi/10.1103/PhysRevLett.134.063002.

[19] Jason L. Evans. "Effect of Ultralight Dark Matter on $g-2$ of the Electron". In: *Phys. Rev. Lett.* 132 (9 Feb. 2024), p. 091801. DOI: 10.1103/PhysRevLett.132.091801. URL: https://link.aps.org/doi/10.1103/PhysRevLett.132.091801.

[20] Michael J. Dugan, Howard Georgi, and David B. Kaplan. "Anatomy of a Composite Higgs Model". In: *Nucl. Phys. B* 254 (1985), pp. 299–326. DOI: 10.1016/0550-3213(85)90221-4.

[21] Shuai Xu and Sibo Zheng. "Resolving muon g-2 anomaly with partial compositeness". In: *Eur. Phys. J. C* 82.10 (2022), p. 969. DOI: 10.1140/epjc/s10052-022-10949-y. arXiv: 2204.05456 [hep-ph].

[22] Manimala Chakraborti, Sven Heinemeyer, and Ipsita Saha. "The new MUON G-2 result and supersymmetry". In: *Eur. Phys. J. C* 81.12 (2021), p. 1114. DOI: 10.1140/epjc/s10052-021-09900-4. arXiv: 2104.03287 [hep-ph].

[23] J. Bailey et al. "New measurement of (g2) of the Muon". In: *Physics Letters B* 55.4 (1975), pp. 420–424. ISSN: 0370-2693. DOI: https://doi.org/10.1016/0370-2693(75)90374-3. URL: https://www.sciencedirect.com/science/article/pii/0370269375903743.

[24] Lorenzo Cotrozzi. "Measurement of the muon anomalous precession frequency with the Run-2/3 data in the Muon $g-2$ experiment at Fermilab". PhD thesis. Pisa U., Mar. 2024.

[25] Richard L. Garwin, Leon M. Lederman, and Marcel Weinrich. "Observations of the Failure of Conservation of Parity and Charge Conjugation in Meson Decays: the Magnetic Moment of the Free Muon". In: *Phys. Rev.* 105 (4 Feb. 1957), pp. 1415–1417. DOI: 10.1103/PhysRev.105.1415. URL: https://link.aps.org/doi/10.1103/PhysRev.105.1415.

[26] Georg Schneider et al. “Double-trap measurement of the proton magnetic moment at 0.3 parts per billion precision”. In: *Science* 358.6366 (2017), pp. 1081–1084. DOI: 10.1126/science.aan0207.

[27] X. Fan, T. G. Myers, B. A. D. Sukra, and G. Gabrielse. “Measurement of the Electron Magnetic Moment”. In: *Phys. Rev. Lett.* 130.7 (2023), p. 071801. DOI: 10.1103/PhysRevLett.130.071801. arXiv: 2209.13084 [physics.atom-ph].

[28] S. Navas et al. “Review of particle physics”. In: *Phys. Rev. D* 110.3 (2024), p. 030001. DOI: 10.1103/PhysRevD.110.030001.

[29] G. Charpak et al. “Measurement of the Anomalous Magnetic Moment of the Muon”. In: *Phys. Rev. Lett.* 6 (3 Feb. 1961), pp. 128–132. DOI: 10.1103/PhysRevLett.6.128. URL: https://link.aps.org/doi/10.1103/PhysRevLett.6.128.

[30] J. Bailey et al. “Precision measurement of the anomalous magnetic moment of the muon”. In: *Physics Letters B* 28.4 (1968), pp. 287–290. ISSN: 0370-2693. DOI: https://doi.org/10.1016/0370-2693(68)90261-X. URL: https://www.sciencedirect.com/science/article/pii/037026936890261X.

[31] Michael E. Peskin and Daniel V. Schroeder. *An Introduction to quantum field theory*. Reading, USA: Addison-Wesley, 1995. DOI: 10.1201/9780429503559.

[32] Colangelo, Gilberto. “Data-driven approaches to the evaluation of hadronic contributions to the (g 2)”. In: *EPJ Web Conf.* 258 (2022), p. 01004. DOI: 10.1051/epjconf/202225801004. URL: https://doi.org/10.1051/epjconf/202225801004.

[33] Yusuke Takeuchi. “Muon g 2/EDM Experiment at J-PARC”. In: *Proceedings of the 24th International Spin Symposium (SPIN2021)*. DOI: 10.7566/JPSCP.37.020603. eprint: https://journals.jps.jp/doi/pdf/10.7566/JPSCP.37.020603. URL: https://journals.jps.jp/doi/abs/10.7566/JPSCP.37.020603.